Obrabotka metallov (tekhnologiya, oborudovanie, instrumenty) = Metal Working and Material Science. 2025 vol. 27 no. 4 pp. 96–115
ISSN: 1994-6309 (print) / 2541-819X (online)
DOI: 10.17212/1994-6309-2025-27.4-96-115

NSTU NETI

Obrabotka metallov - Metal Working and Material Science

Journal homepage: http://journals.nstu.ru/obrabotka_metallov

Evaluation of the melting ability of oxide fluxes in A-TIG welding of carbon and low-alloy steels

Antonina Karlina [1, a*], ***Viktor Kondratiev*** [2, 3, b], ***Vitaly Gladkikh*** [1, c], ***Galina Vitkina*** [3, d], ***Roman Kononenko*** [4, e]

[1] National Research Moscow State University of Civil Engineering, 26 Yaroslavskoe Shosse, Moscow, 129337, Russian Federation
[2] A.P. Vinogradov Institute of Geochemistry of the Siberian Branch of the Russian Academy of Sciences, 1A Favorsky str., Irkutsk, 664033, Russian Federation
[3] Cherepovets State University, 5 Lunacharsky pr., Cherepovets, 162600, Russian Federation
[4] Irkutsk National Research Technical University, 83 Lermontova str., Irkutsk, 664074, Russian Federation

[a] https://orcid.org/0000-0003-3287-3298, karlinat@mail.com; [b] https://orcid.org/0000-0002-7437-2291, imz@mail.ru;
[c] https://orcid.org/0000-0003-1953-1584, gladkich_87@mail.ru; [d] https://orcid.org/0000-0002-1076-2709, 20procents@mail.ru;
[e] https://orcid.org/0009-0001-5900-065X, istu_politeh@mail.ru

ARTICLE INFO

Article history:
Received: 14 September 2025
Revised: 07 October 2025
Accepted: 23 October 2025
Available online: 15 December 2025

Keywords:
Welding
Activating fluxes
Penetration depth
Coating thickness

ABSTRACT

Introduction. Tungsten inert gas (*TIG*) welding has gained widespread popularity due to its advantages, including effective shielding, a stable arc, easy heat input adjustment, reduced metal spatter, and an attractive weld appearance. However, relatively shallow penetration and low efficiency limit its application. To improve welding efficiency and expand its scope of application, researchers both domestically and internationally have conducted significant studies aimed at increasing the energy density of the traditional TIG arc. This includes activating *TIG* (*A-TIG*) arc welding, which utilizes a flux applied to the weld surface. Further investigation of the mechanism for increasing arc energy density in *A-TIG* welding will allow us to propose new ideas and methods for highly efficient *TIG* welding technology. **The purpose** of this study is to evaluate the technological potential of using oxide activators TiO_2 and SiO_2 to improve penetration efficiency and weld quality of carbon and low-alloy steels. **Methods.** This work involved comparative *A-TIG* welding tests. The tests included the use of 3.5 mm and 8 mm thick plates (300 mm × 300 mm) made of unalloyed (carbon) steel *St3* and low-alloy steel 0.09 *C-2Mn-Si*. Welding tests included the use of single-component fluxes in the form of oxides (TiO_2, SiO_2). All experimental welds were performed under the same conditions, without the use of filler metal (*TIG* welding), with a current in the range of 10–200 A and a welding speed of 150 mm/min. Arc voltage was maintained in the range of 10.4 V to 12.8 V; heat input was in the range of 0.499 kJ/mm to 0.614 kJ/mm. All welds were subjected to visual inspection of the surface condition and macrostructural studies to determine their dimensions. **Results and discussion.** Most tests observed significant differences in arc shape compared to traditional *TIG* and *A-TIG* processes. Results of *A-TIG* welding tests on unalloyed and low-alloy steels showed that penetration depth increased slightly in steels characterized by a higher degree of deoxidation and metallurgical purity. Evidently, not every activator was responsible for the increased penetration depth, but the use of TiO_2 and SiO_2 oxides was undoubtedly beneficial. An arc constriction mechanism is proposed, which is widely applicable to *A-TIG* welding of steel with various types of fluxes studied. Arc constriction occurs due to the formation of negative ions in the outer region of the arc or due to the flux coating on the surface. Thus, arc constriction increases the current density and heat intensity at the root of the anode. This increases the force and pressure of magnetic constriction, resulting in a strong downward convection flow. The use of silicon and titanium oxides (TiO_2 and SiO_2) increases penetration depth during *A-TIG* welding, regardless of steel type and grade. The degree of penetration increase was limited to a range of 40% to 200%.

For citation: Karlina A.I., Kondratiev V.V., Gladkikh V., Vitkina G., Kononenko R.V. Evaluation of the melting ability of oxide fluxes in A-TIG welding of carbon and low-alloy steels. *Obrabotka metallov (tekhnologiya, oborudovanie, instrumenty) = Metal Working and Material Science*, 2025, vol. 27, no. 4, pp. 96–115. DOI: 10.17212/1994-6309-2025-27.4-96-115. (In Russian).

Introduction

Welding is the preferred method for joining different grades of steel, allowing for strong, continuous joints with superior corrosion resistance compared to bolt or rivet joints. *TIG* (tungsten inert gas) or *GTA* (gas tungsten arc) welding is often used due to its precision and excellent weld quality. It uses an electric arc

*** Corresponding author**
Karlina Antonina I., Ph.D. (Engineering), Research Associate
National Research Moscow State University of Civil Engineering,
26 Yaroslavskoe Shosse,
129337, Moscow, Russian Federation
Tel: +7 950 120-19-50, **e-mail:** karlinat@mail.ru

and an inert gas (such as argon) to protect the weld pool from contamination. This method is highly effective for thin or fragile materials, providing low deformation, excellent control, and a polished surface, making it suitable for applications in machine parts and mechanisms that require both strength and precision.

Despite its advantages, *TIG* welding has limitations, especially in terms of weld penetration depth. Typically, *TIG* welding of stainless steels in argon environments limits full weld penetration to seams no thicker than 3 mm and relatively low welding speeds. Although welding speeds can be significantly increased (up to 160%) by using helium or helium-argon mixtures with hydrogen additions as shielding gas, the weld penetration depth increases only slightly (1–2 mm) [1–3]. The ability to improve penetration by selecting a protective mixture is further limited by the need to use inert or weakly reducing gases, which limits the choice to argon and helium and their mixtures.

As mentioned above, a single pass of butt joints with square edges provides a penetration of about 3 mm, which leads to the need for additional passes for thicker materials, increasing the welding time and cost. Additional passes generate even more heat, expanding the heat-affected zone (*HAZ*) and potentially altering both the metallurgical and microstructural characteristics of the weld. Thicker components require wider root gaps and more filler material, resulting in increased material consumption and welding time [1–3].

Preparing the edges for *TIG* welding, especially for thick materials, is a time-consuming and laborious process. The *ISO 9692-1:2013* standard requires beveling or grooving the edges to reduce the thickness of the weld at the root, ensuring sufficient penetration. However, this procedure increases the labor intensity, welding time, and overall costs [1–5].

To eliminate these limitations, the technology of activated *TIG* welding (*A-TIG*) was developed, which involves applying a thin layer of activating flux (usually oxides or halides in combination with solvents such as acetone or ethanol) to the base material before welding [1, 2]. *A-TIG* welding (*A-GTAW*) with activated flux is a welding method that was first used at the E. O. Paton Institute of Electric Welding, Ukraine, in the late 1950s and early 1960s [1–3]. Initially, the *A-TIG* method was used for welding titanium, then for welding high-strength martensitic steels ($\boldsymbol{R}_m \approx 1{,}500$ MPa), and finally for welding stainless steels [3–10].

The free-burning argon arc is compressed into a plasma arc through mechanical, thermal, and magnetic compression. The energy density of the plasma arc is 1–2 orders of magnitude higher than that of a conventional free-burning arc, making plasma arc welding *(PAW*) one of the three high-energy-density welding methods. The arc compression mechanism provides a new method for increasing the energy density of the TIG arc. Based on this mechanism, many methods have been developed to increase the energy density of the TIG arc. These include activating *TIG* arc welding (*A-TIG*), double-electrode *TIG* welding (*DE-TIG*), keyhole *TIG* welding (*K-TIG*), high-frequency pulse *TIG* welding (*H-TIG*), hybrid *TIG* arc welding with ultrasound (*U-TIG*), magnetic field controlled *TIG* welding (*M-TIG*), and hollow tungsten electrode negative pressure arc welding (*HWP-TIG)*.

In recent years, researchers [3–19] have paid great attention to the *A-TIG* welding technology of various metals and alloys. Many research articles by domestic and foreign authors have been published on TIG welding of steel with various activated fluxes and their combinations [8–25].

Many authors [8–16] have investigated the effect of five different oxide fluxes, MnO_2, TiO_2, MoO_3, SiO_2, and Al_2O_3, on weld geometry changes, microstructural behavior, and hardness changes during *TIG* welding of 6–8 mm thick stainless steel. All fluxes, with the exception of Al_2O_3, increase weld penetration due to a combined effect of the reverse *Marangoni* effect and arc constriction, thereby reducing the angular deformation of the welded joints. In addition, the SiO_2 flux facilitated the penetration of the root pass. The difficulty in dissolving aluminum oxide leads to a lack of arc constriction, resulting in a shallow weld in the case of Al_2O_3. Another study was conducted [16] on stainless steel using SiO_2, TiO_2, Cr_2O_3, and CaO fluxes. They also noted that the SiO_2 flux had the most significant impact on penetration and proposed a mechanism for arc constriction for deeper penetration.

The authors of [16–22] analyzed the microstructure, mechanical properties, and corrosion resistance of *A-TIG* welds, which revealed the mechanism for improving the microstructure of *A-TIG* welds.

In [5–9, 18–22], the composition of a composite nanoparticle-based activator was developed and optimized, further clarifying the relationship between the activator and the formation and quality of the weld. Many studies [4–16] have shown that most activators can significantly compress the arc, increase the penetration depth, and reduce the width of the weld bead.

According to studies [17–22], it is not clear whether the *Marangoni* effect in the molten pool is the main reason for increased penetration, but arc compression is not an inevitable phenomenon in *A-TIG*. Some activators can compress the arc, while others do not affect the arc state. However, arc compression will inevitably lead to increased arc energy density.

The effect of activating fluxes Cr_2O_3, TiO_2, SiO_2, Fe_2O_3, NaF, and AlF_3, both individually and as binary fluxes such as SiO_2-TiO_2, has been studied in many articles [5–29], where the depth of penetration was used as a criterion for evaluation. In some cases, activating fluxes (especially oxides) have a positive effect on the depth of penetration, increasing it by 40–50% [15–25], while in other cases, they have a negligible effect [4, 5, 30–38]. This is due to the fact that most of the studies [15–39] have been conducted under various conditions of the welding process (current value, arc voltage, welding speed, coating thickness, type of binder used in the preparation of the flux, particle size of the flux, etc.). According to the authors [1, 2], all of these factors will affect the penetration capability of the welding arc and, as a result, the effectiveness and application of the activating flux.

The purpose of the work is to evaluate the penetration capability of *A-TIG* welding using TiO_2 and SiO_2 oxide fluxes on carbon and low-alloy steels. To achieve this purpose, the following ***tasks*** were solved during the research:

– determination of technological parameters of the *A-TIG* welding process using TiO_2 and SiO_2 oxide fluxes (current value, coating thickness, welding speed) affecting the penetration capability;

– conducting metallographic studies of welds during *A-TIG* welding using TiO_2 and SiO_2 oxide fluxes;

– conducting visualized studies of the process using photo documentation of individual stages of the process.

Research methods and materials

For the experiments, plates of dead-melted steel *St3* (*ASTM A283* Grade C**)** with dimensions of 5500 mm × 100 mm and thicknesses of 3, 5, 8, 10, 12, and 25 mm, as well as low-alloy steel 0.9% *C*-2% *Mn*-1% *Si*, were used. The welding tests included the use of single-component fluxes in the form of oxide powders (TiO_2, SiO_2), with particle sizes of 40 and 80 micrometers, produced by *Real-Dzerzhinsk LLC*, Russia. The components were ground in a ceramic mortar and then sieved through a laboratory sieve with a mesh size of 0.056 mm. Before application, the powder was mixed with a fast-evaporating liquid (acetone) to create a paste-like suspension. The prepared flux was then applied to the surface of the plates using a brush. This method of applying the activating flux is currently used in most studies related to the *A-TIG* process. A bonding varnish and double-sided conductive tape were also used. To achieve consistent flux thickness and minimize the impact of this factor on the test results, the paste consistency was kept constant. The coating thickness was monitored using a *TP-34* thickness gauge based on an eddy current transducer. The methodology adopted for the experimental work is presented in Fig. 1.

All experimental welds were performed under the same conditions, without the use of filler metal (autogenous *TIG* welding), with a current range of 10–200 A and a welding speed of 150 mm/min. The arc voltage was in the range of 10.4 V to 12.8 V, and the linear energy input was in the range of 0.499 kJ/mm to 0.614 kJ/mm. The welding experiments were conducted using a *TIG 250P AC/DC* welding machine, which consists of a *TIG* welding power supply, a welding fixture, a *TIG* torch, and an argon cylinder. The *TIG* welding equipment has a current range of 10 to 200 A, an open-circuit voltage of 75 to 85 V, a frequency of 50/60 Hz, and forced air cooling. The **arc** length (distance between the tungsten electrode and the workpiece), the welding speed, and the welding current are the most influential variables that require optimal control to obtain accurate and repeatable experimental results. The welding fixture was developed in-house to securely hold the torch and workpiece and accurately control the welding speed and the arc

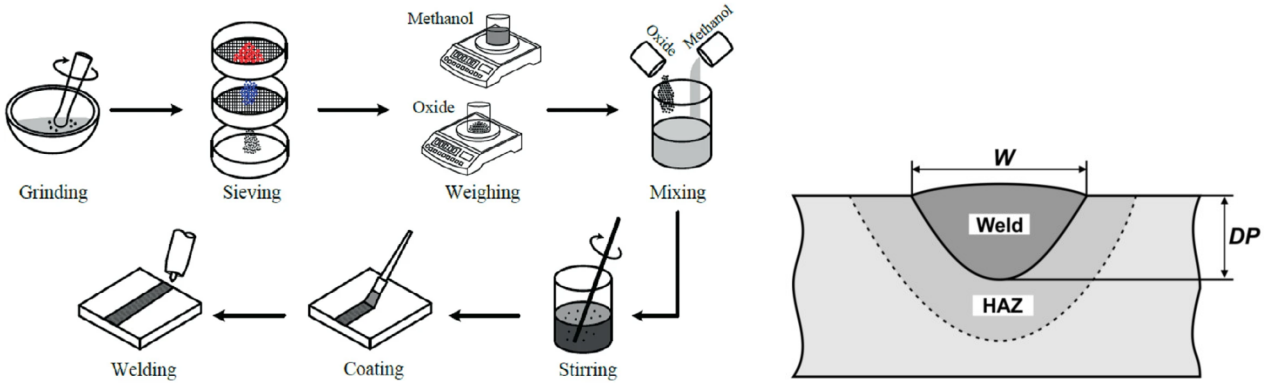

a *b*

Fig. 1. Methodology [29] for the preparation of activating fluxes:

a – weld parameters; *b* – (***W*** – weld width; ***DP*** – penetration depth; ***HAZ*** – heat-affected zone; ***Weld*** – weld)

length during welding. It holds the base plate for welding and sets the desired welding speed between 40 and 200 mm/min. The flow rate of the shielding argon was maintained between 10 L/min and 15 L/min. A tungsten electrode (ø 2.4 mm) doped with thorium oxide (grade *WT20* according to *EN ISO 6848*) was used. All welds were subjected to visual inspection of the surface condition and macro-structural studies to determine their dimensions. Samples for macrostructural studies were cut, mounted, ground, polished and etched with a 4% *Nital* reagent. The width of the welds was measured every 10 mm along the entire length of the welds. For statistical processing of the results, 3 experiments were carried out for each welding condition, then the results were averaged.

Samples for macrostructural studies were selected from the central part of the weld. The arc burning process was recorded by a digital *SLR* camera -*á SONY 350* and a high-speed camera *PCO.1200s* according to the method described in [15]. A *Tektronix TDS-1012B* digital oscilloscope was used to measure current and voltage.

Research results

The results of macrostructural tests of welds performed on the respective steel grades using various activated fluxes (TiO_2, SiO_2) are presented in Figs. 2–4, and the results of measurements of the penetration depth and weld width are presented in Table 1.

Macroscopic images of weld geometry at 50× magnification are shown in Fig. 2 with calibrated measurements of weld penetration and weld width. The weld penetration depth, weld bead width, and weld depth-to-width (***D***/***W***) ratio are three key metrics that describe the geometric characteristics of welds.

The geometric characteristics of the *A-TIG* welds obtained with the selected combinations of current, speed, and flux are shown in Table 1 and Figs. 2 and 3. The penetration depth and bead width of the *A-TIG* weld varied significantly depending on the flux and application method parameters. Different combinations of flux and application method resulted in variations in penetration depth and bead width compared to the conventional *TIG* process. The effect of increasing the penetration depth for a given welding current is clearly visible when an activated flux is used during the welding process (Table 1, Figs. 2–4).

The experiments showed that the maximum penetration depth is achieved at high welding currents during *A-TIG* welding, but the increase in penetration depth is limited for conventional *TIG* welding, as shown in Fig. 4.

An increase in current also leads to a wider weld bead (Fig. 4). The flux layer thickness has a strong effect on the weld penetration, as a thicker flux layer can increase the weld penetration. The weld penetration depends on the welding current, but the optimal flux layer thickness is crucial for a high-quality weld. Fig. 5 shows the weld penetration as a function of coating thickness, and Fig. 6 shows the weld penetration as a function of steel chemical composition.

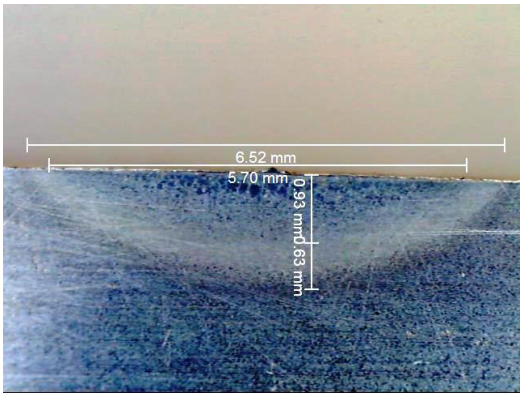

a

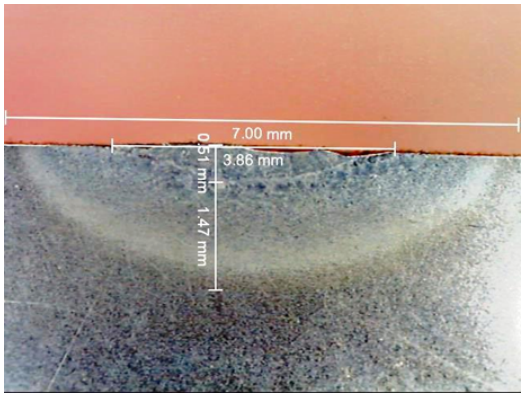

b

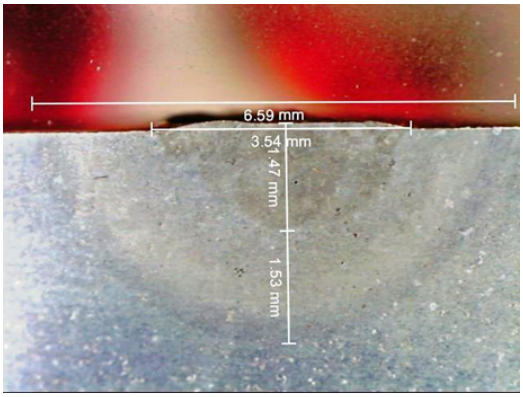

c

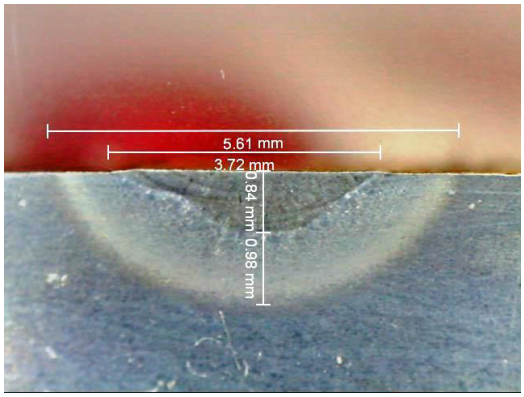

d

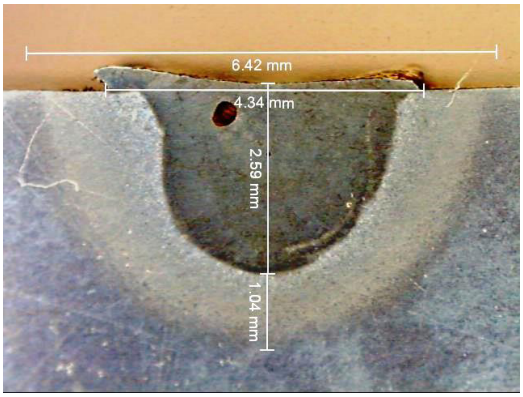

e

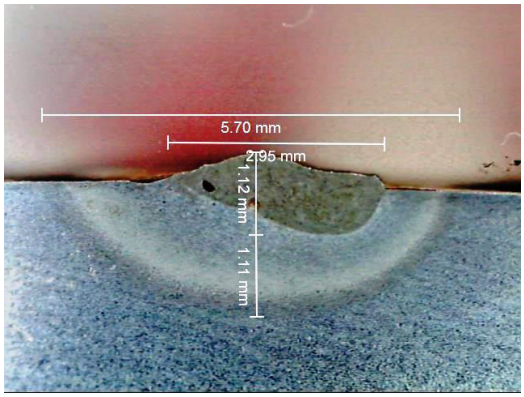

f

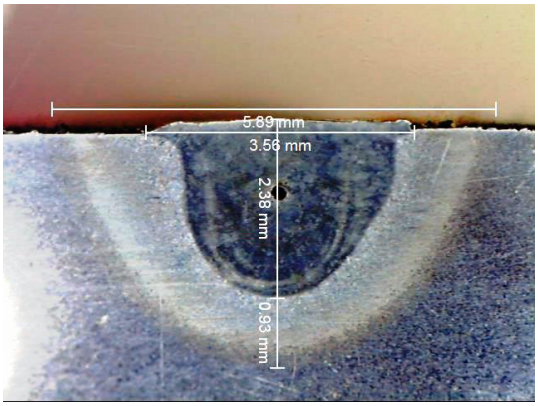

g

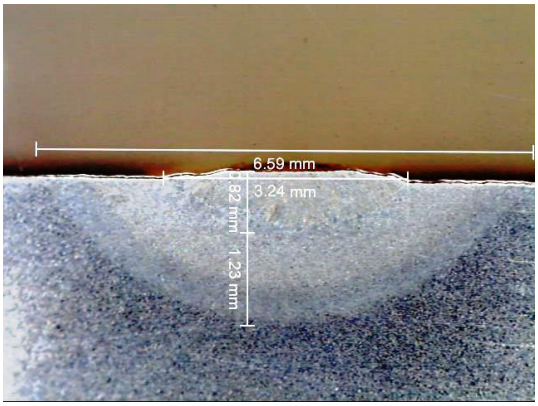

h

Fig. 2. Cross sections of steel:
a – without flux and without surface melting (current 100 A); *b* – without flux and with surface melting (current 120 A); *c* – silicon oxide (current 120 A); *d* – titanium oxide (current 120 A); *e* – silicon oxide (current 150 A); *f* – titanium oxide (current 150 A); *g* – silicon oxide (current 160 A); *h* – titanium oxide (current 160 A)

The influence of the composition of activating fluxes of different particle size on the width and depth of penetration

Current, A	Flux applied to *St3* steel	Depth of penetration, mm	Penetration width, mm
100	Without flux	1.15	5.3
100	SiO_2 0.04 mm particle size (double-sided conductive tape, bonding varnish)	1.64	5.37
100	SiO_2 0.08 mm particle size (bonding varnish)	2.66	5.35
100	SiO_2 0.04 mm particle size (bonding varnish)	2.52	4.98
100	SiO_2 0.08 mm particle size (double-sided conductive tape and bonding varnish)	1.2	4.3
100	**Aerosil®** (bonding varnish)	1.96	1.96

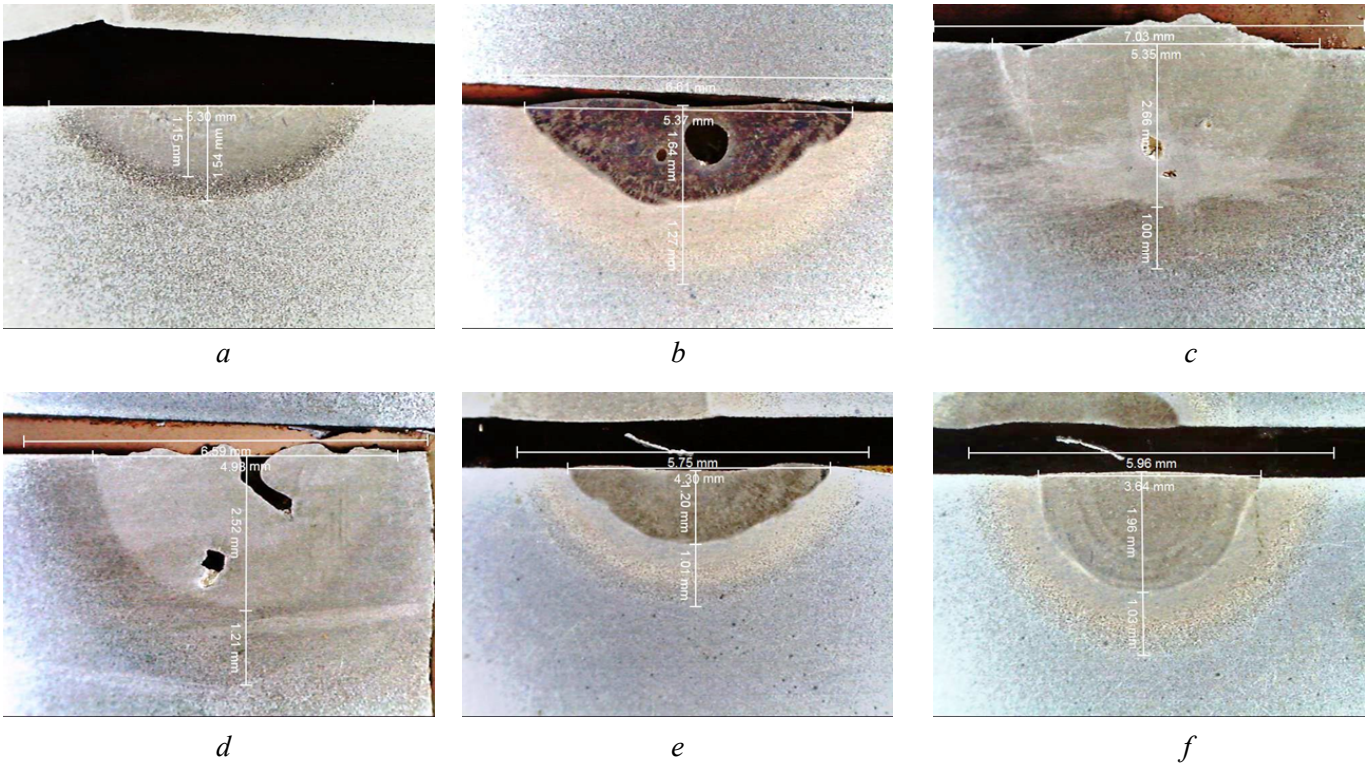

a *b* *c*

d *e* *f*

Fig. 3. Cross sections (current 100A):
a – without flux; *b* – SiO_2 0.04 (double-sided conductive tape, bonding varnish); *c* – SiO_2 0.08 (bonding varnish); *d* – SiO_2 0.04 (bonding varnish); *e* – SiO_2 0.08 (double-sided conductive tape, bonding varnish); *f* – *Aerosil* (bonding varnish)

Figs. 7–10 below show photographs of the melting process of different types of activating fluxes on the surface of *St3* steel during conventional *TIG* and *A-TIG* welding. The welding process without flux is visualized in Fig. 7. A diffuse combustion mode of the welding arc without distinct anode and cathode spots is visible. The arc column has a conical (bell-shaped) form.

Fig. 8 shows the welding process with a 0.08 mm layer of SiO_2 flux applied using acetone as a carrier. It can be seen that the intense vaporization of the activating flux causes the arc column to constrict, resulting in a more concentrated anode region directed towards the cathode. The electric arc enters a constricted (or focused) attachment mode, forming a concentrated anode spot.

The heating time of the surface with the activated flux applied was increased compared to the heating of the surface without the activated flux. This leads to a constriction of the arc column and a deviation of

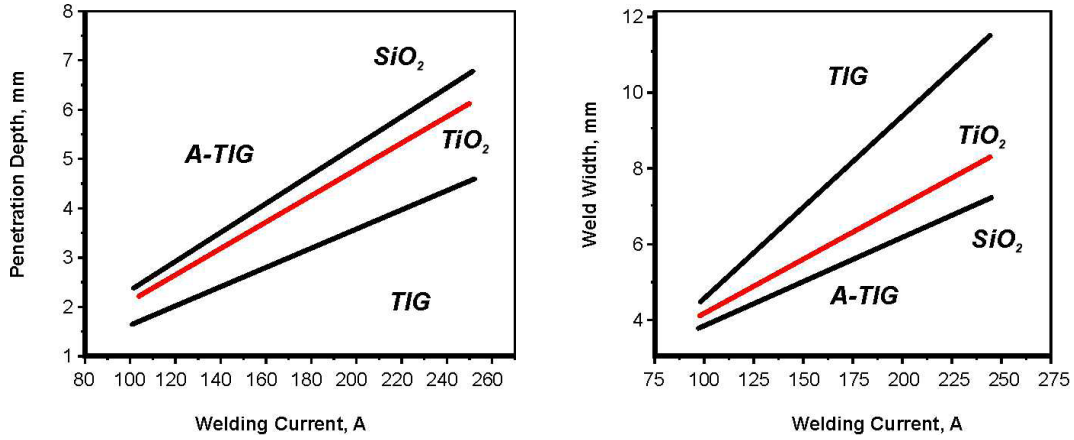

Fig. 4. Change in the geometric dimensions of the melting zone on a steel *St3* plate, 20 mm thick (penetration depth and weld width) with changing current during *TIG* and *A-TIG* welding

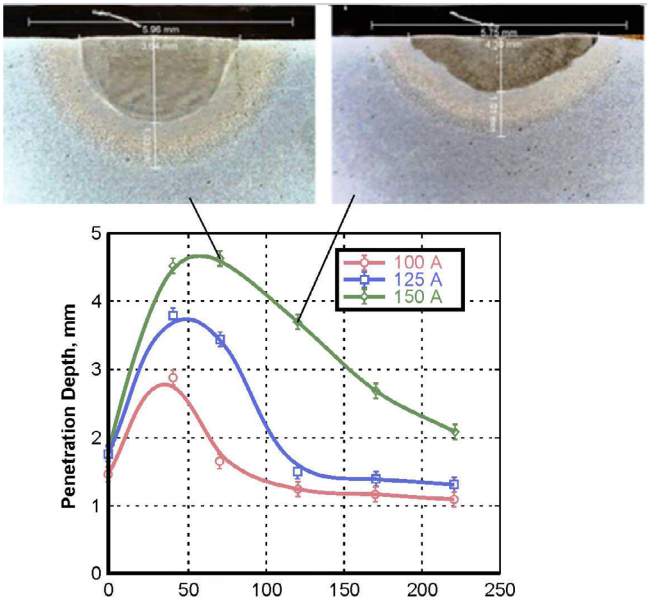

Fig. 5. Effect of changing coating thickness on penetration depth

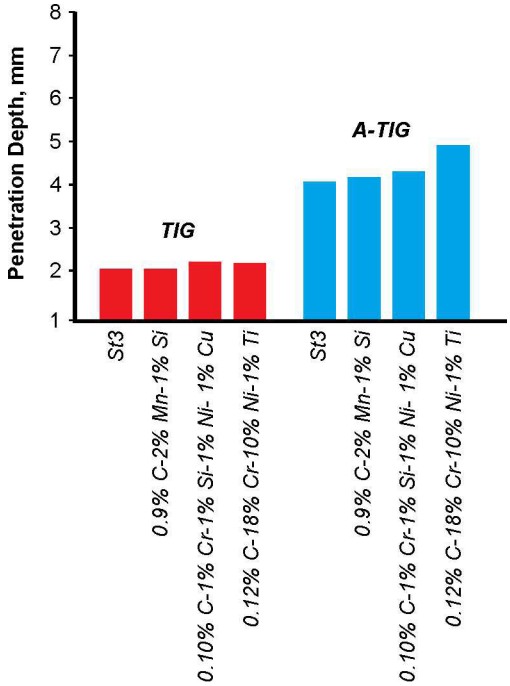

Fig. 6. Dependence of penetration depth on chemical composition of steel (plate thickness 10 mm, current 200 A)

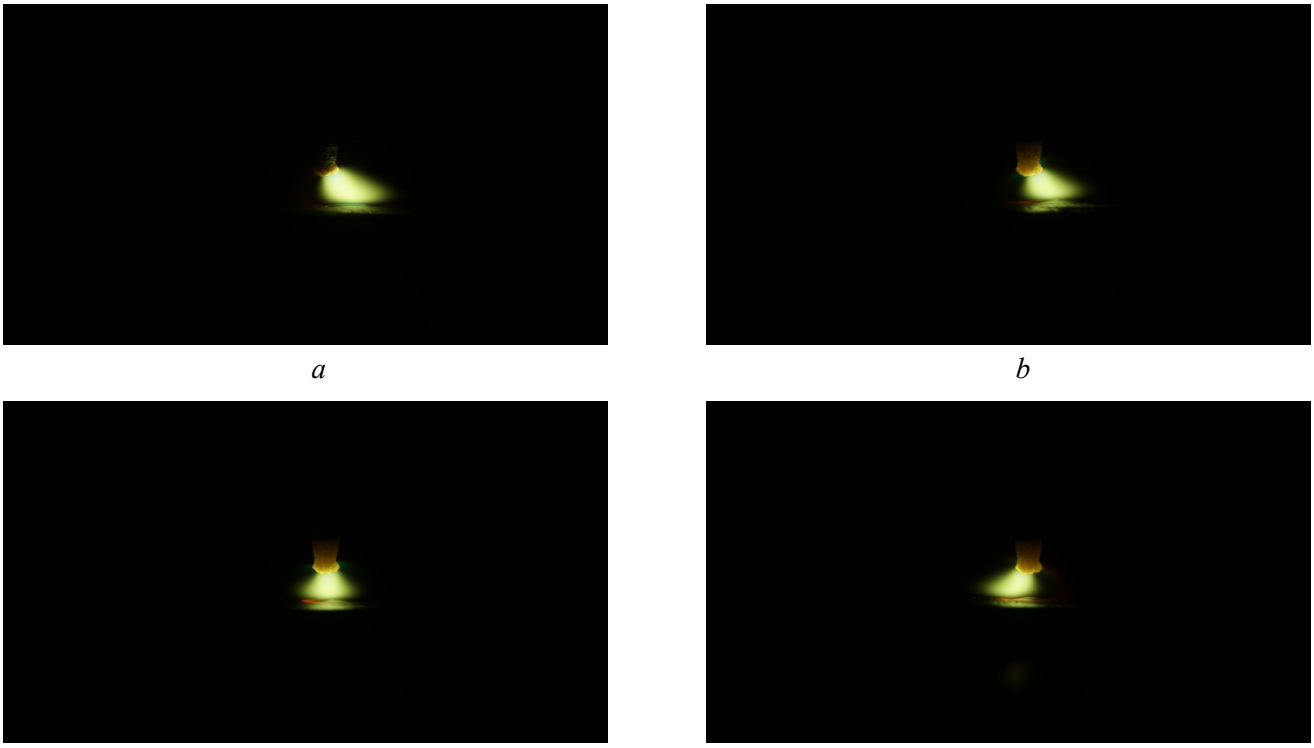

a *b*

c *d*

Fig. 7. The process of welding steel-3 without flux:
a, *b*, *c*, *d* – stages of movement of the welding arc along the sample

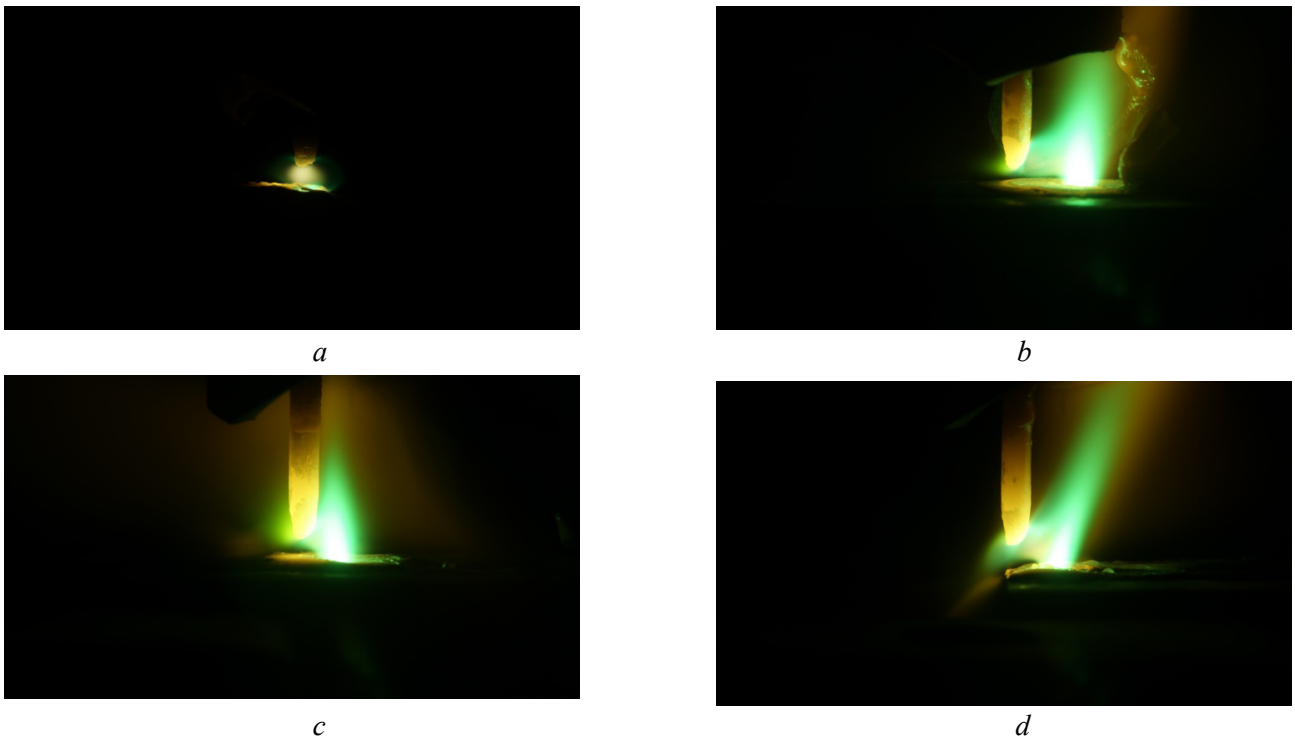

a *b*

c *d*

Fig. 8. The process of welding steel *St3* with applied flux SiO_2, particle size 0.08 mm, using acetone as a binder:
a, *b*, *c*, *d* – stages of movement of the welding arc along the sample

the anode spot from the arc axis. This causes an increase in the arc length and, as a result, an increase in the arc voltage, which is accompanied by an increase in the effective arc power (***P***=***U***×***I***). The same situation is presented in Fig. 9, which shows photographs of the melting process of the activated flux SiO_2 with a particle size of 0.08 mm using a bonding varnish.

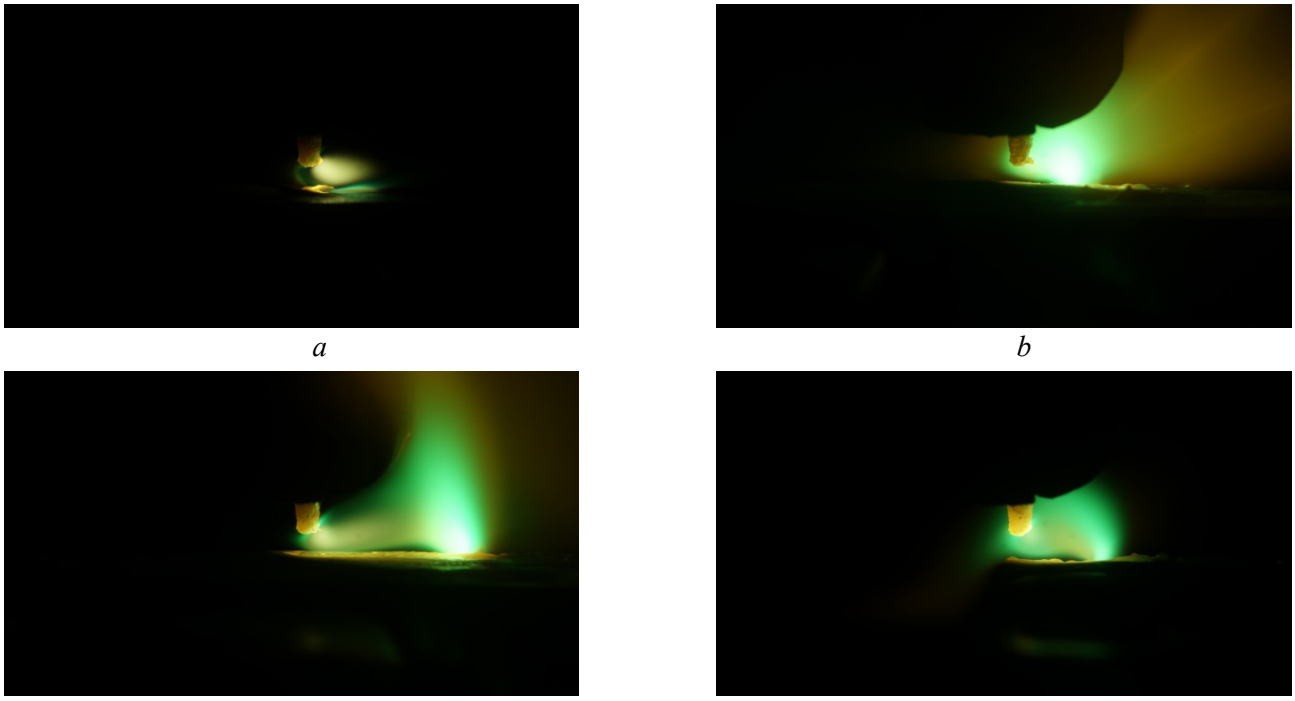

a *b*

c *d*

Fig. 9. The process of welding steel *St3* with applied flux SiO_2 particle size 0.08 mm using a bonding varnish:

a, *b*, *c*, *d* – stages of movement of the welding arc along the sample

Fig. 10 shows photographs of the process of melting the SiO_2 activating flux with a particle size of 0.04 mm using a bonding varnish. Similarly to the 0.08 mm fraction, the heating time of the surface with the activated flux applied compared to the heating of the surface without the activated flux increased,

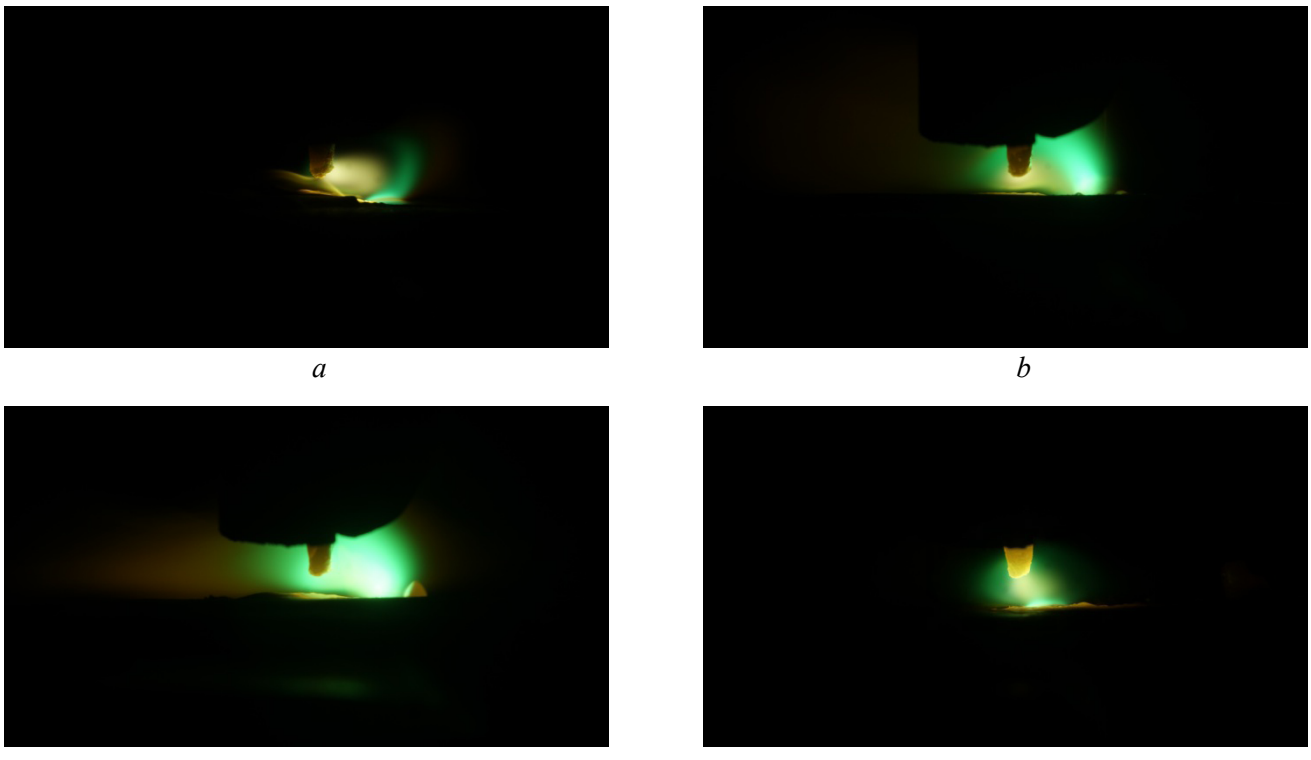

a *b*

c *d*

Fig. 10. The process of welding steel *St3* with applied flux with TiO_2 particle size of 0.04 mm using a bonding varnish:

a, *b*, *c*, *d* – stages of movement of the welding arc along the sample

which led to the arc column constriction and the anode spot deviating from the axis of the column moving at a speed of 3.3 mm/sec. At the initial moment of arc ignition, the column has a typical spatial position; after 0.24 seconds, intensive vaporization of the activating flux begins and the arc column constricts, a more concentrated anode region appears, directed towards the cathode. The anode region length is 20–30 % greater than for the 0.08 mm fraction. The noted features of vaporization **o**f activating fluxes and the behavior of the arc column in Fig. 8–10 are also observed for other flux compositions.

Fig. 11 shows the oscillograms of the arc burning process without flux and with flux. It can be seen that the arc burning over the flux layer has higher voltage values due to the constricted mode of arc attachment.

Fig. 12 shows the welding process of *St3* steel samples with TiO_2 flux, which is applied in a 1.5 mm thick layer using a bonding varnish, and a 0.5 mm thick layer in Fig. 13.

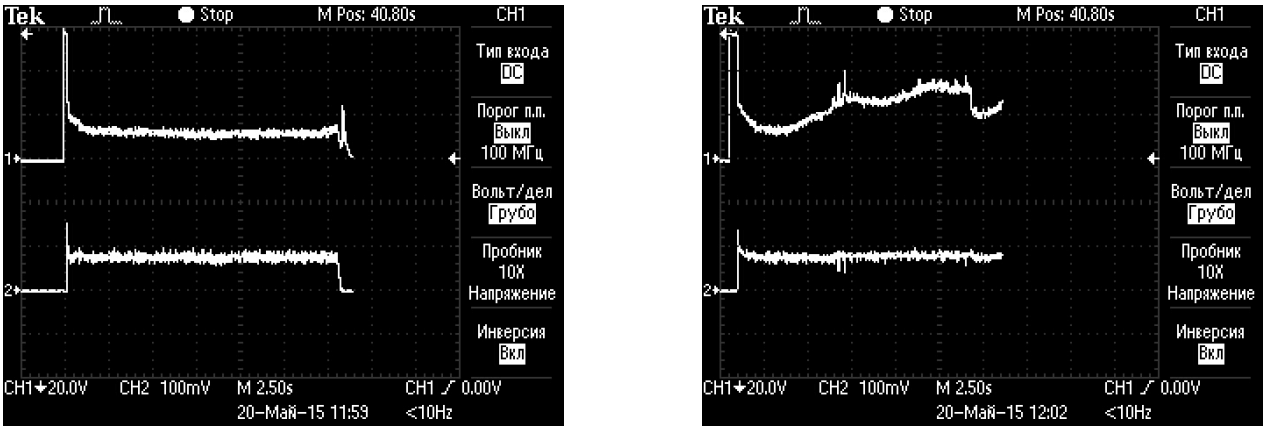

a *b*

Fig. 11. Oscillograms of current and voltage of the welding arc:

a – without flux; *b* – with flux

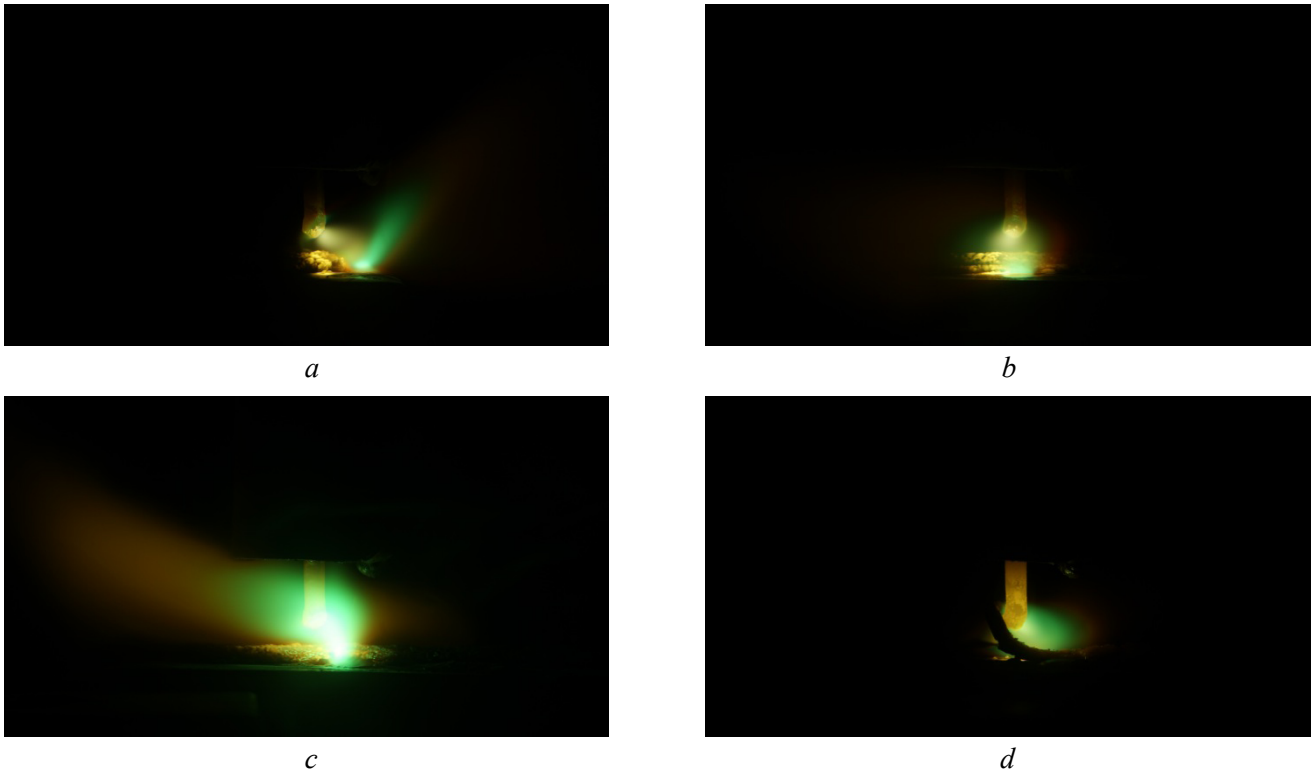

a *b*

c *d*

Fig. 12. The process of welding steel *St3* with TiO_2 applied in a 1.5 mm layer using a bonding varnish:

a, *b*, *c*, *d* – stages of movement of the welding arc along the sample

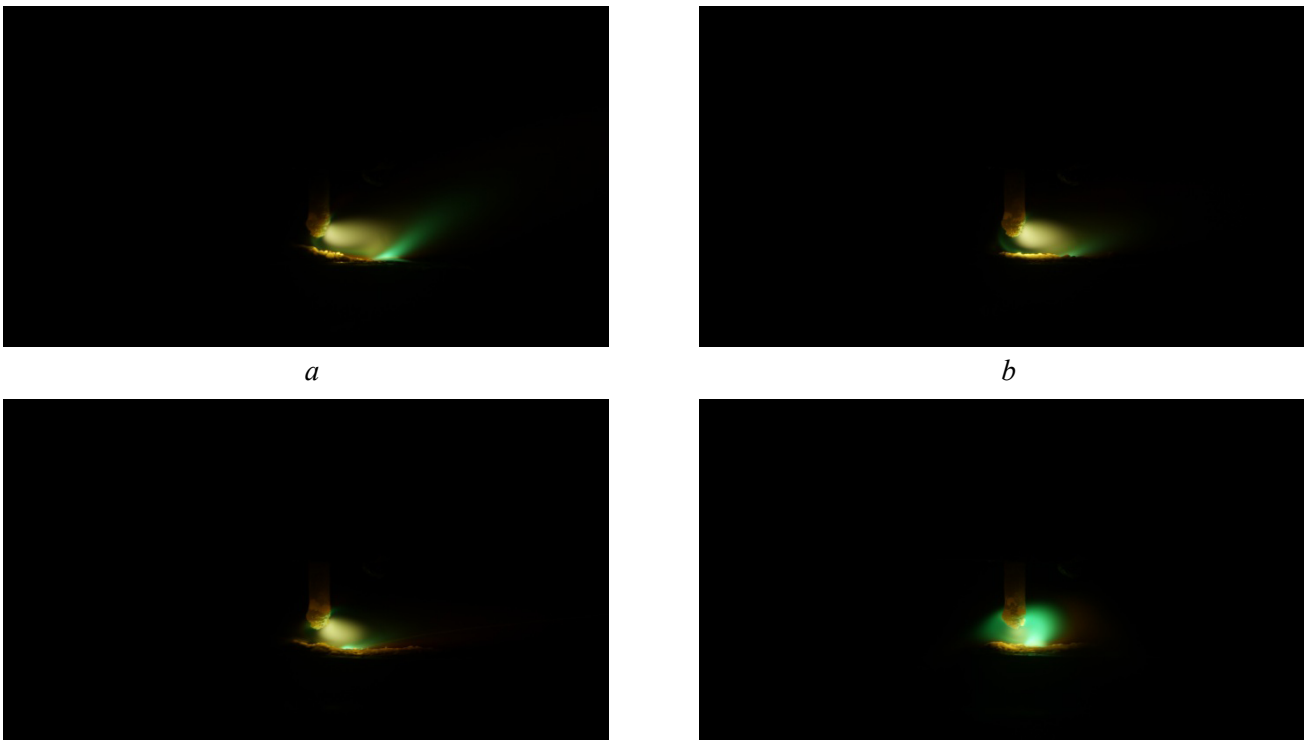

a *b* *c* *d*

Fig. 13. The process of welding steel *St3* with TiO_2 C flux applied in a 0.05 mm layer using a bonding varnish: *a*, *b*, *c*, *d* – stages of movement of the welding arc along the sample

The results of the experiments show that the penetration depth increased in almost all cases where activating flux was applied. A comparison of the effect of activated fluxes on the penetration depth during *A-TIG* welding of low-alloy steels and stainless steel revealed a similar effect of TiO_2 and SiO_2 oxides on both groups of steels. The effect of oxides, or rather the oxygen supplied by the oxides to the weld pool, can be explained by Marangoni convection, as has been reported in many scientific publications [3–29].

Arc images obtained during some tests are presented. In most tests, there were no significant differences in the arc shape compared to the conventional *TIG* process. In some tests using SiO_2 flux, the electric arc exhibited a tendency to deviate forward. This type of flux also caused the most significant changes in arc voltage, which were at least twice as high as those observed with other fluxes.

It is observed that the flux layer thickness has a very strong effect on the weld penetration (Fig. 5). The weld penetration initially increases linearly with the flux layer thickness up to 50–70 μm, and then shows a downward trend (Fig. 5). The Conventional *TIG* weld penetration corresponds to zero coating thickness and ranges from 1.4 to 1.9 mm for the investigated welding currents of 100 to 150 A. Depending on the welding current, the maximum penetration in *A-TIG* is achieved for a flux layer thickness of 40 to 70 μm. The observed maximum weld penetration values are 4.8 mm, 3.9 mm, and 2.9 mm, respectively, for welding currents of 150, 125, and 100 A. The optimal thickness appears to increase with increasing welding current. For example, the maximum penetration depth is achieved at about 40 μm at 100 A and about 70 μm at 150 A. Thus, the optimization of flux layer thickness depends on the heat input of the welding arc.

When the flux layer thickness exceeds the optimal value, the penetration is significantly reduced. This rapid decrease can be explained by the higher energy consumption required to overcome the flux barrier. Silicon dioxide is essentially a non-conductive material, providing high electrical resistance to the arc. A stable arc can only be established once the flux becomes liquid or is completely removed through vaporization. As the energy consumption for this effect increases with the flux layer thickness, the proportion of the incident energy that is effectively utilized for creating the weld pool decreases significantly.

In addition, as the flux layer thickness increases, the electric arc becomes unstable due to the unmelted flux, which provides higher electrical resistance on the advancing side. This causes a change in the arc pro-

file, which then stretches back towards the molten pool (Fig. 7–9). This lagging effect becomes increasingly important as the flux layer thickness increases for a given current or as the welding current decreases for a given thickness. Even with an optimal flux layer thickness of about 50 μm (Fig. 7–9), the lagging effect is observed when comparing TIG and A-TIG video frames. The lagging effect is associated with the higher electrical resistance of silicon oxide, which decreases with increasing temperature, especially when it enters the liquid phase. Since melting occurs at a higher temperature on the advancing side, the arc tends to lag behind the tip of the tungsten electrode. This arc lag increases the effective arc length and partially contributes to the increased arc voltage, as described later in this paper.

In the *A-TIG* process, there is an improvement in **the depth-to-width (*D*/*W*)** ratio, which is achieved through the combined effect of arc constriction and "reverse" *Marangoni* convection, also known as surface tension-induced convection or thermocapillary convection. In Marangoni convection, when the activating flux is applied to the workpiece, it delivers surface-active elements (e.g., oxygen) to the weld pool. This changes the surface tension gradient to become positive ($d\gamma/dT > 0$), and the oxygen content therefore affects the flow of the liquid in the weld pool [5].

The relationship between surface tension and temperature has been studied in [6–21]. It has been found that when welding low-sulfur and low-oxygen steel, the surface tension decreases with increasing temperature, resulting in a negative surface tension gradient. This leads to a radially outward flow in the weld pool. This phenomenon is discussed in detail in [22]. The authors believe that concentrations of surfactants above 50 ppm affect the direction and magnitude of thermocapillary forces [22], which changes the surface tension gradient in the weld pool from negative to positive [6–12].

The flow in the weld pool occurs from a region of higher surface tension (cooler liquid weld pool) to a region of lower surface tension (warmer liquid weld pool), causing the molten metal on the upper surface to flow outwards. However, in the presence of surface-active elements like oxygen, this gradient reverses, causing an inward flow towards the center. This internal flow results in deeper penetration and a narrower weld bead. This change in the direction of the surface tension gradient explains the change in the direction of the Marangoni flow.

In the arc constriction mechanism, the electron affinity (electronegativity) of the flux plays an important role [6, 7]. The arc, which exists on the surface of the flux-coated workpiece, produces a large number of positive ions at the temperature of the arc column [4]. It can be concluded that electrons are absorbed by the flux vapors around the weld pool, resulting in a decrease in the number of charged particles present in the arc. The highly electronegative vapor pushes the arc column inward in a radial direction. The resulting ions attract the free electrons present in the arc column, creating a constriction of the arc, and the base metal melts, promoting deeper penetration [5–22].

The electromagnetic *Lorentz* force also contributes to increasing the ***D*/*W*** ratio in the A-*TIG* mechanism. As the welding current increases, the magnitude of the *Lorentz* force increases. The smaller the radius of the arc root, the higher the *Lorentz* force [18–20]. The greater *Lorentz* force acts vertically downward in the center of the molten weld pool and increases the penetration. The electromagnetic *Lorentz* force and Marangoni force control the convection of the weld pool and increase the ***D*/*W*** ratio. The weld pool experiences driving forces such as buoyancy, aerodynamic shear stress, and plasma-induced reaction forces on the surface. All of them effectively improve the penetration in the *A-TIG* process, but their role is minimal compared to the *Marangoni* force, and therefore they can be neglected in the micro-scale analysis.

The research conducted has shown that the geometry of the weld is certainly influenced by variable parameters that must be precisely controlled to achieve the best weld quality. Some of these parameters that affect the *A-TIG* process are discussed below.

Many studies have shown [5–26] that the vaporization/decomposition of flux depends on the rate of its reaction, which in turn depends on the specific surface area of the particles. Therefore, it has been experimentally established [5–22] that flux particles with a size of 0.8 to 4 μm improve the penetration of the weld. However, this effect is not observed when using larger particles (25 μm) because they have a lower vaporization rate. Smaller flux particles have a higher specific surface area compared to larger particles, which results in better vaporization [12]. As the flux layer thickness increases, so does the heat required to

overcome the flux barrier, which reduces the depth of penetration at a given current value. Although it is known that penetration depends on the welding current, the optimal flux layer thickness is still important for achieving a high-quality weld [4–16].

It is important to understand that before applying a flux layer, it is converted into a paste by mixing the powdered flux with a suitable solvent, which must be evaporated before the welding process begins. Acetone and alcohol are the most commonly used carriers. Experiments have shown that acetone is the solvent that provides the best results, resulting in maximum penetration [10–14]. However, many studies do not pay close attention to the influence of the solvent type, which may affect the results obtained.

The welding current directly affects the geometric characteristics of the weld, such as the cross-sectional area, width, and depth of penetration. When comparing conventional *TIG* and *A-TIG* welding, there is almost a twofold difference in the depth of penetration when the current is increased. For conventional *TIG* welding with higher current values, the increase in weld width is very slight, while it increases significantly for *A-TIG* welding.

Increasing the welding speed leads to a decrease in the heat input to the weld and results in a shallower weld. The depth of penetration is inversely proportional to the welding speed at a given welding current.

The arc energy density is directly dependent on the arc length, which is a critical factor in *A-TIG* welding [3–9]. Generally, shorter arcs are preferred to prevent the dissipation of arc heat into the environment and to ensure that the maximum arc heat is transferred to the workpiece. However, a minimum distance must be maintained to ensure arc stability and minimize electrode contamination [5–12]. For *A-TIG* welding of stainless steel, a 2-4 mm arc length is typically used [4–6].

When maintaining a constant travel speed and welding current and using an activating flux, there is a slight increase in arc voltage. It is known that the flux vapors attract electrons during vaporization, which leads to a constriction of the arc and an increase in voltage. The degree of increase depends primarily on the composition of the oxide flux. Experiments have clearly shown that there is an obvious correlation between the measured arc voltage and the resulting arc constriction, so higher voltage values will result in a more pronounced arc constriction, as confirmed by other authors [16–29].

Experiments by various authors [1–8] show that the depth of penetration depends on the oxygen content in the weld pool during welding, as it contributes to the development of reverse *Marangoni* convection. The oxygen content can be precisely controlled by using a suitable flux composition and optimizing the welding parameters [1, 2].

Research by various authors shows [5–7] that the addition of nitrogen to the shielding gas increases arc energy and has a positive effect on the geometry and properties of the weld [22–29]. For example, the depth of penetration and cross-sectional area of the weld increase when nitrogen is added to an argon environment [26–31]. Angular deformation is also minimized when nitrogen is added, as it is directly related to the width of the weld, and nitrogen promotes complete penetration, which reduces angular deformation [24–28]. It has been found that hardness, tensile strength, and resistance to hot cracking can increase significantly when nitrogen is added [27–29].

It is known [1–6] that hydrogen-based shielding gas has high thermal conductivity at temperatures close to the dissociation of hydrogen molecules. Therefore, the addition of hydrogen has a significant impact on the volume of molten material in the weld pool [26–29]. An increase in arc voltage, penetration depth, melting efficiency, heat input, and cross-sectional area has been observed, while oxide formation tends to be reduced when hydrogen is added [5–7, 10–16].

Conclusions

The main results can be summarized as follows:

1. The use of silicon and titanium oxides (TiO_2 and SiO_2) increased the weld penetration depth during *A-TIG* welding, regardless of the type and grade of steel. The increase in weld penetration depth ranged from 30% to more than 200%.

2. The flux layer thickness is an important parameter in *A-TIG* welding. This study shows significant variations in the weld penetration for a thickness range of 0–200 μm. It has been found that the optimized

thickness in the *A-TIG* process ranges from 40 to 70 μm, depending on the welding current, and results in a twofold increase in weld penetration at a given current level.

3.. The welding current directly affects the geometric characteristics of the weld when using TiO_2 and SiO_2 fluxes, such as the cross-sectional area, width, and depth of the weld. When comparing conventional *TIG* and *A-TIG* welding, there is almost a twofold difference in the depth of penetration for the same increase in current.

4. The effect of the type and grade of steel on the penetration capability when using activating fluxes has not been clearly identified. Only minor changes in the depth of penetration have been recorded between low-alloy and stainless steels.

References

1. Paton B.E., Zamkov V.N., Prilutsky V.P., Poritsky P.V. Kontraktsiya dugi flyusom pri svarke vol'framovym elektrodom v argone [Arc contraction by flux during tungsten electrode welding in argon]. *Avtomaticheskaya svarka = Automatic Welding*, 2000, no. 1, pp. 3–9.

2. Savitsky M.M., Kushnirenko B.N., Oleynik O.N. Osobennosti svarki stalei vol'framovym elektrodom s aktiviruyushchimi flyusami [Features of welding steels with a tungsten electrode with activating fluxes]. *Avtomaticheskaya svarka = Automatic Welding*, 1999, no. 12, pp. 18–22.

3. Acharya S., Patra S., Das S. Predicting A-TIG weld bead geometry of 304 stainless steel using artificial neural networks. *Discover Mechanical Engineering*, 2025, vol. 4 (1), p. 12. DOI: 10.1007/s44245-025-00096-5.

4. Modenesi P.J. The chemistry of TIG weld bead formation. *Welding International*, 2015, vol. 29 (10), pp. 771–782. DOI: 10.1080/09507116.2014.932990.

5. Mohsein Z.H., Abdulwahhab A.B., Abbas A.M. Study effect of active flux on mechanical properties of TIG welding process. *Results in Engineering*, 2025, vol. 26, p. 104681. DOI: 10.1016/j.rineng.2025.104681.

6. Görgün E. Advancing welding quality through intelligent TIG welding: A hybrid deep learning approach for defect detection and quality monitoring. *Dicle Üniversitesi Mühendislik Fakültesi Mühendislik Dergisi*, 2025, vol. 16 (3), pp. 677–685. DOI: 10.24012/dumf.1642978.

7. Morisada Y., Fujii H., Xukun N. Development of simplified active flux tungsten inert gas welding for deep penetration. *Materials & Design*, 2014, vol. 54, pp. 526–530. DOI: 10.1016/j.matdes.2013.08.081.

8. Dhandha K.H., Badheka V.J. Effect of activating fluxes on weld bead morphology of P91 steel bead-on-plate welds by flux assisted tungsten inert gas welding process. *Journal of Manufacturing Processes*, 2015, vol. 17, pp. 48–57. DOI: 10.1016/j.jmapro.2014.10.004.

9. Nayee S.G., Badheka V.J. Effect of oxide-based fluxes on mechanical and metallurgical properties of dissimilar activating flux assisted-tungsten inert gas welds. *Journal of Manufacturing Processes*, 2014, vol. 16 (1), pp. 137–143. DOI: 10.1016/j.jmapro.2013.11.001.

10. Shravan C., Radhika N., Deepak Kumar N.H., Sivasailam B. A review on welding techniques: properties, characterisations and engineering applications. *Advances in Materials and Processing Technologies*, 2023, vol. 10, pp. 1126–1181. DOI: 10.1080/2374068X.2023.2186638.

11. Mi H., Ma J., Feng L., Guo W., He B. A critical review on advanced welding technologies to fabricate test blanket modules and irradiation damage behaviour of the welded joints in nuclear fusion applications. *Journal of Manufacturing Processes*, 2025, vol. 141, pp. 829–864. DOI: 10.1016/j.jmapro.2025.03.025.

12. Fande A.W., Taiwade R.V., Raut L. Development of activated tungsten inert gas welding and its current status: A review. *Materials and Manufacturing Processes*, 2022, vol. 37 (8), pp. 841–876. DOI: 10.1080/10426914.2022.2039695.

13. Tanaka M., Shimizu T., Terasaki T., Ushio M., Koshiishi F., Yang C.-L. Effects of activating flux on arc phenomena in gas tungsten arc welding. *Science and Technology of Welding and Joining*, 2000, vol. 5 (6), pp. 397–402. DOI: 10.1179/136217100101538461.

14. Babkin A.S., Kotov N.S., Terekhov V.V. Vliyanie aktiviruyushchikh flyusov na kharakteristiki elektricheskoi dugi i kachestvo shvov pri svarke austenitnykh stalei [The influence of activating fluxes on the characteristics of the electric arc and the quality of seams in welding austenitic steels]. *Izvestiya TulGU. Tekhnicheskie nauki = Bulletin of Tula State University. Technical Sciences*, 2022, no. 10, pp. 507–514. DOI: 10.24412/2071-6168-2022-10-507-514.

15. Ivanchik N.N., Balanovsky A.E., Kondratyev V.V., Tyutrin A.A. Issledovaniya produktov pererabotki otkhodov kremniya v kachestve ul'tradispersnykh aktiviruyushchikh flyusov dlya dugovoi svarki [Research of silicon waste processing products as ultradispersed activating fluxes for arc welding]. *Zhurnal Sibirskogo federal'nogo*

universiteta. Tekhnika i tekhnologii = Journal of Siberian Federal University. Engineering and Technologies, 2018, no. 11 (2), pp. 155–167. DOI: 10.17516/1999-494X-0019.

16. Parshin S.G. *Nanostrukturirovannye i aktiviruyushchie materialy dlya dugovoi svarki* [Nanostructured and activating materials for arc welding]. St. Petersburg, Polytechnic University Publ., 2020. DOI: 10.18720/SPBPU/2/si20-888.

17. Jayakrishnan S., Chakravarthy P. Flux bounded tungsten inert gas welding for enhanced weld performance – A review. *Journal of Manufacturing Processes*, 2017, vol. 28, pp. 116–130. DOI: 10.1016/j.jmapro.2017.05.023.

18. Bhanu V., Gupta A., Pandey C. Role of A-TIG process in joining of martensitic and austenitic steels for ultra-supercritical power plants-a state of the art review. *Nuclear Engineering and Technology*, 2022, vol. 54 (8), pp. 2755–2770. DOI: 10.1016/j.net.2022.03.003.

19. Pandya D., Badgujar A., Ghetiya N. A novel perception toward welding of stainless steel by activated TIG welding: a review. *Materials and Manufacturing Processes*, 2021, vol. 36 (8), pp. 877–903. DOI: 10.1080/10426914.2020.1854467.

20. Kumar N., Pandey C., Kumar P. Dissimilar welding of Inconel alloys with austenitic stainless-steel: a review. *Journal of Pressure Vessel Technology*, 2023, vol. 145 (1), p. 011506. DOI: 10.1115/1.4055329.

21. Martyushev N.V., Skeeba V.Yu. The method of quantitative automatic metallographic analysis. *Journal of Physics: Conference Series*, 2017, vol. 803 (1), p. 012094. DOI: 10.1088/1742-6596/803/1/012094.

22. Kavishwar S., Bhaiswar V., Kochhar S., Fande A. Comprehensive studies on conventional and novel weld cladding techniques and their variants for enhanced structural integrity: an overview. *Welding International*, 2024, vol. 38 (9), pp. 618–638. DOI: 10.1080/09507116.2024.2402285.

23. Sharma P., Dwivedi D.K. A-TIG welding of dissimilar P92 steel and 304H austenitic stainless steel: Mechanisms, microstructure and mechanical properties. *Journal of Manufacturing Processes*, 2019, vol. 44, pp. 166–178. DOI: 10.1016/j.jmapro.2019.06.003.

24. Efremenkov E.A., Martyushev N.V., Skeeba V.Yu., Grechneva M.V., Olisov A.V., Ens A.D. Research on the possibility of lowering the manufacturing accuracy of cycloid transmission wheels with intermediate rolling elements and a free cage. *Applied Sciences*, 2022, vol. 12 (1), p. 5. DOI: 10.3390/app12010005.

25. Vidyarthy R.S., Dwivedi D.K., Vasudevan M. Influence of M-TIG and A-TIG welding process on microstructure and mechanical behavior of 409 ferritic stainless steel. *Journal of Materials Engineering and Performance*, 2017, vol. 26 (3), pp. 1391–1403. DOI: 10.1007/s11665-017-2538-5.

26. Zhang R.H., Pan J.L., Katayama S. The mechanism of penetration increase in A-TIG welding. *Frontiers of Materials Science*, 2011, vol. 5, pp. 109–118. DOI: 10.1007/s11706-011-0125-5.

27. Singh S.R., Khanna P. A-TIG (activated flux tungsten inert gas) welding: – A review. *Materials Today: Proceedings*, 2021, vol. 44, pp. 808–820. DOI: 10.1016/j.matpr.2020.10.712.

28. Wu H., Chang Y., Mei Q., Liu D. Research advances in high-energy TIG arc welding. *The International Journal of Advanced Manufacturing Technology*, 2019, vol. 104 (1), pp. 391–410. DOI: 10.1007/s00170-019-03918-5.

29. Tseng K.H., Lin P.Y. UNS S31603 stainless steel tungsten inert gas welds made with microparticle and nanoparticle oxides. *Materials*, 2014, vol. 7 (6), pp. 4755–4772. DOI: 10.3390/ma7064755.

30. Mamadaliev R.A., Bakhmatov P.V., Martyushev N.V., Skeeba V.Yu., Karlina A.I. Influence of welding regimes on structure and properties of steel 12KH18N10T weld metal in different spatial positions. *Metallurgist*, 2022, vol. 65 (11–12), pp. 1255–1264. DOI: 10.1007/s11015-022-01271-9.

31. Balanovskiy A.E., Astafyeva N.A., Kondratyev V.V., Karlina A.I. Study of mechanical properties of C-Mn-Si composition metal after wire-arc additive manufacturing (WAAM). *CIS Iron and Steel Review*, 2021, vol. 22, pp. 66–71. DOI: 10.17580/cisisr.2021.02.12.

32. Karlina A.I., Karlina Y.I., Kondratiev V.V., Kononenko R.V., Breki A.D. Study of wear of an alloyed layer with chromium carbide particles after plasma melting. *Crystals*, 2023, vol. 13 (12), p. 1696. DOI: 10.3390/cryst13121696.

33. Kolosov A.D., Gozbenko V.E., Shtayger M.G., Kargapoltsev S.K., Balanovskiy A.E., Karlina A.I., Sivtsov A.V., Nebogin S.A. Comparative evaluation of austenite grain in high-strength rail steel during welding, thermal processing and plasma surface hardening. *IOP Conference Series: Materials Science and Engineering*, 2019, vol. 560, p. 012185. DOI: 10.1088/1757-899X/560/1/012185.

34. Malushin N.N., Gizatulin R.A., Martyushev N.V., Valuev D.V., Karlina A.I., Kovalev A.P. Strengthening of metallurgical equipment parts by plasma surfacing in nitrogen atmosphere. *Metallurgist*, 2022, vol. 65 (11–12), pp. 1468–1475. DOI: 10.1007/s11015-022-01292-4.

35. Nokhrina O.I., Gizatulin R.A., Golodova M.A., Proshunin I.E., Valuev D.V., Martyushev N.V., Karlina A.I. Alloying and modification of iron-carbon melts with natural and man-made materials. *Metallurgist*, 2022, vol. 65 (11–12), pp. 1429–1448. DOI: 10.1007/s11015-022-01289-z.

36. Yelemessov K., Baskanbayeva D., Martyushev N.V., Skeeba V.Y., Gozbenko V.E., Karlina A.I. Change in the properties of rail steels during operation and reutilization of rails. *Metals*, 2023, vol. 13, p. 1043. DOI: 10.3390/met13061043.

37. Skeeba V.Yu., Ivancivsky V.V., Kutyshkin A.V., Parts K.A. Hybrid processing: the impact of mechanical and surface thermal treatment integration onto the machine parts quality. *IOP Conference Series: Materials Science and Engineering*, 2016, vol. 126 (1), p. 012016. DOI: 10.1088/1757-899x/126/1/012016.

Conflicts of Interest

The authors declare no conflict of interest.